RSC Advances

PAPER

View Article Online
View Journal | View Issue

Cite this: *RSC Adv.*, 2018, **8**, 15030

An electrochemical anodization strategy towards high-activity porous MoS_2 electrodes for the hydrogen evolution reaction†

Xuerui Mao,[a] Tianliang Xiao,[a] Qianqian Zhang[b] and Zhaoyue Liu *[a]

Received 21st February 2018
Accepted 12th April 2018

DOI: 10.1039/c8ra01554f

rsc.li/rsc-advances

Molybdenum disulfide (MoS_2) is a promising non-precious metal electrocatalyst for the hydrogen evolution reaction (HER). Herein, we have described an anodization route for the fabrication of porous MoS_2 electrodes. The active porous MoS_2 layer was directly formed on the surface of a Mo metal sheet when it was subjected to anodization in a sulfide-containing electrolyte. The Mo sheet served as both a supporter for MoS_2 electrocatalysts and a conductive substrate for electron transport. After optimizing the anodization parameters, the anodized MoS_2 electrode showed a high electrocatalytic activity with an onset potential of −0.18 V (*vs.* RHE) for the HER, a Tafel slope of ~101 mV per decade and an overpotential of 0.23 V at a current density of 10 mA cm^{-2} for the HER. These results indicate that our facile anodization strategy is an efficient route towards a high-activity MoS_2 electrode.

1. Introduction

Hydrogen is considered to be an ideal energy carrier because of its cleanliness and renewability. The electrochemical achievement of the hydrogen evolution reaction (HER), when using precious metals, means that it is one of the most efficient technologies used to produce hydrogen.[1] Due to the rarity and high cost of precious metals, the development of non-precious metal materials for the HER is therefore necessary.[2–5] MoS_2, a typical non-precious electrocatalyst for the HER, has recently attracted significant attention because of its low cost and excellent catalytic activity.[6,7] MoS_2 electrodes have been developed *via* the immobilization of MoS_2 nanoparticles or nanosheets onto various conductive substrates using methods such as chemical vapor deposition,[8–12] high-temperature sulfurization,[13–18] solvothermal/hydrothermal synthesis,[19–27] chemical exfoliation,[28–31] electrodeposition,[32–34] and photocatalytic reactions.[35] However, these methods always require a high temperature, extreme pressure, complex precursors or a long reaction time. The development of an alternative route towards MoS_2 electrodes is of significant importance.

Electrochemical anodization is a versatile method for the deposition of functional materials onto the surface of metal substrates. Due to the variability of the components, *i.e.* metal substrate and electrolyte, electrochemical anodization can be used to fabricate various functional oxides or non-oxides facilely. For example, nanotubular or nanoporous structures of TiO_2,[36–39] Fe_2O_3,[40,41] WO_3,[42–44] Ta_2O_5,[45–48] MoO_x (ref. 10, 49 and 50) and CdS[51] have been reported and they were formed *via* anodization of the corresponding metal in the optimized electrolyte. Considering that the electrocatalyst needs to be fixed onto a conductive substrate for the HER, electrochemical anodization is a very suitable route towards MoS_2 electrodes.

Herein, we have reported the fast synthesis of porous MoS_2 electrocatalysts on pure Mo metal *via* electrochemical anodization at room temperature and ambient pressure. The Mo metal served as both a molybdenum source and a conductive substrate for MoS_2. The resulting MoS_2 electrocatalysts were immobilized on the surface of Mo metal sheets, which could be used as electrodes for the HER directly. After optimizing the anodization parameters, the anodized MoS_2 electrode exhibited a high electrocatalytic activity for the HER.

2. Experimental section

2.1 Synthesis of MoS_2 electrodes *via* electrochemical anodization

The porous MoS_2 electrode was prepared *via* one-step anodization in a two-electrode electrochemical cell using platinum foil as a cathode. The anode was a pure Mo sheet (Alfa Aesar), which acted as the Mo source. Before anodization, the Mo sheet was sonicated in acetone, isopropanol and deionized water in sequence. The electrolyte was 0.2 M Na_2S (Xilong Chemicals, China) aqueous solution, which served as the sulfur source. The

[a]*Key Laboratory of Bio-Inspired Smart Interfacial Science and Technology of Ministry of Education, School of Chemistry, Beihang University, Beijing 100191, P. R. China. E-mail: liuzy@buaa.edu.cn; Tel: +86-10-82317801*

[b]*Key Laboratory of Micro-nano Measurement, Manipulation and Physics of Ministry of Education, School of Physics and Nuclear Energy Engineering, Beihang University, Beijing 100191, P. R. China*

† Electronic supplementary information (ESI) available. See DOI: 10.1039/c8ra01554f

thickness of the anodized MoS_2 layer was controlled by altering the anodization parameters, such as voltage and reaction time.

2.2 Materials characterization

The morphology of the anodized MoS_2 layer was investigated using a FEI Quanta FEG 250 environmental scanning electron microscope (SEM) and a FEI JEM-1200EX transmission electron microscope (TEM). The energy dispersive X-ray spectra (EDX) of the MoS_2 electrode were obtained using a JSM-7500F field-emission scanning electron microscope (JEOL, Japan) coupled with an INCA Energy 250 energy spectrum analyzer. The chemical composition of the MoS_2 layers was investigated using a Thermo escalab 250XI X-ray Photoelectron Spectrometer (XPS). The amorphous phase of the anodized MoS_2 layer was confirmed by measurement of the X-ray diffraction patterns (XRD, Bruker D8 FOCUS X-ray diffractometer).

2.3 Electrochemical measurements

The electrocatalytic activity of the anodized MoS_2 electrodes for the HER was studied by measuring their polarization curves in 0.5 M N_2-purged H_2SO_4 solution using a three-electrode electrochemical configuration. The Tafel curves were calculated from the polarization curves. The anodized MoS_2 electrode with a geometric area of 1 cm^2 was used as a working electrode. The reference electrode was Ag/AgCl in 3.5 M KCl and the counter electrode was a platinum wire. The polarization potentials were obtained using a CHI660D electrochemical workstation (Shanghai Chenhua Apparatus Co., China) with a scan rate of 5 mV s^{-1}. The polarization potential was calibrated against a reversible hydrogen electrode (RHE) based on the following equation: φ (*vs.* RHE) = φ (*vs.* Ag/AgCl) + 0.205 V. Electrochemical impedance spectroscopy (EIS) was carried out in 0.5 M H_2SO_4 solution at a potential of −0.2 V (*vs.* RHE). The frequency range was from 100 kHz to 0.01 Hz.

3. Results and discussion

During electrochemical anodization, the Mo metal acted as a Mo source and the sulfide ion in the electrolyte served as a sulfur source for MoS_2. When a positive voltage is applied to a Mo metal in Na_2S electrolyte, the Mo metal will be oxidized to Mo^{4+}, which subsequently reacts with S^{2-} to form MoS_2 on the metal surface as follows:

$$Mo \rightarrow Mo^{4+} + 4e$$

$$Mo^{4+} + 2S^{2-} \rightarrow MoS_2$$

When the Mo sheet was anodized at 2.0 V for 10 min, the metallic luster of the Mo sheet disappeared and a uniform black MoS_2 layer was formed (Fig. 1a). The anodized MoS_2 layer demonstrated a micro-/nano-structured surface that consisted of some nanosized particles (80–107 nm) on microsized MoS_2 blocks (1.7–2.3 μm) (Fig. 1b). Energy dispersive X-ray spectroscopy (EDX) revealed the existence of Mo and S elements in the particles and blocks from the overlapped characteristic peaks of Mo and S at ~2.3 keV (Fig. S1†). The cross-sectional image (Fig. 1c) indicates that the interior of the MoS_2 layer shows a porous structure, which might result from the localized dissolution of Mo metal into the electrolyte during anodization. The thickness of the MoS_2 layer was determined to be about 1.2 μm. The porous structure of the MoS_2 layer was further confirmed from the TEM measurement, which indicated that there were some nanopores in the anodized MoS_2 layer (Fig. 1d).

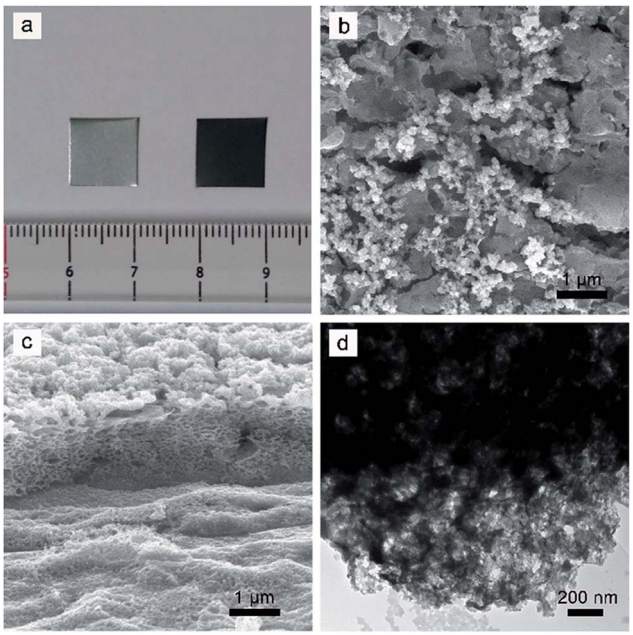

Fig. 1 (a) Photographs of the Mo sheet before and after anodization. After anodization, a uniform black MoS_2 layer was formed. (b) Top view and (c) cross-sectional SEM image of the anodized MoS_2 layer. The surface of the MoS_2 layer demonstrated a micro-/nano-structure and the interior showed a porous structure. (d) A TEM image of the anodized MoS_2 layer, indicating that there were some nanopores in the interior of the MoS_2 layer.

The valences of the molybdenum and sulfur elements in the anodized layer were investigated using X-ray Photoelectron Spectroscopy (XPS). The spectra of the molybdenum 3d orbitals revealed a mixture of Mo oxidation states (Fig. 2a). After peak fitting, the two peaks at 229.3 eV and 232.4 eV were assigned to the $3d_{5/2}$ and $3d_{3/2}$ orbitals, respectively, for the +4 oxidation state.[10,52] The peaks at 235.5 eV and 233.5 eV indicate the existence of the higher +6 oxidation states, probably due to the formation of MoO_3 during the process of anodization.[52,53] The peak at 230.3 eV was ascribed to the original Mo metal.[53] From the spectrum of the sulfur 2p orbital (Fig. 2b), a single doublet at 161.8 eV and 162.8 eV could be observed, which was ascribed to the S $2p_{3/2}$ and $2p_{1/2}$ orbitals of S^{2-}, respectively.[10,54,55] The peaks at 163.5 eV and 164.7 eV indicated the existence of bridging S_2^{2-}.[54–57] The small peak at 168.0 eV corresponds to the binding energy of sulfur in a sulfate ion,[52,58,59] which might result from the oxidation of S^{2-} during anodization. The X-ray diffraction patterns (XRD) showed that no resolved diffraction peaks could be detected except for the peaks for the Mo metal

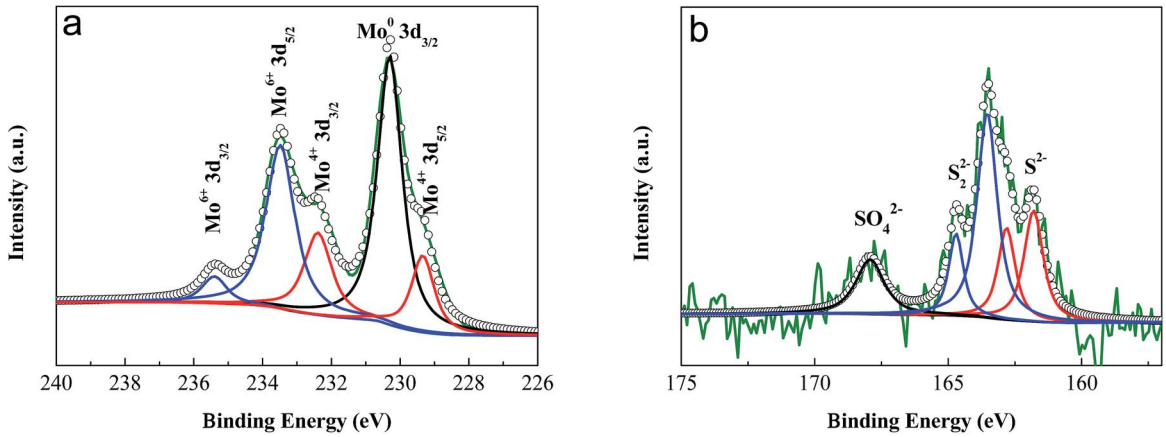

Fig. 2 XPS spectra of (a) Mo 3d and (b) S 2p orbitals in the anodized MoS_2 layer. The two peaks at 229.3 eV and 232.4 eV were assigned to the $3d_{5/2}$ and $3d_{3/2}$ orbitals of Mo^{4+}, respectively. The characteristic peaks at 161.8 eV and 162.8 eV were ascribed to the S $2p_{3/2}$ and $2p_{1/2}$ orbitals of S^{2-}, respectively.

and Al supporter, indicating an amorphous phase for the anodized MoS_2 layer (Fig. 3). The very weak diffraction peaks at 10–30° may be indexed to MoO_3.

The thickness of the anodized MoS_2 layer could be controlled by altering the anodization parameters, such as voltage and reaction time. As shown in Fig. 4a, when the anodization time was fixed at 10 min, the thickness of the MoS_2 layer increased from ~280 nm to ~2.0 μm along with the increase in voltage from 1.5 to 3.0 V (Fig. S2†). The visible color of the anodized MoS_2 layer changed from light brown to black. Note that when the anodization voltage was lower than 2.5 V, the MoS_2 layer was fixed onto the Mo substrate tightly. However, when the voltage reached 3.0 V, the MoS_2 layer became loose and easily detached from the substrate. Furthermore, if the anodization voltage remained at 2.5 V, the increase in the reaction time from 5 to 20 min led to an increase in the thickness of the MoS_2 layer from ~1.2 μm to ~2.8 μm (Fig. 4b and S2†). The visible color of the anodized MoS_2 layer remained almost unchanged. Our results indicate clearly that the thickness of the MoS_2 layer could be controlled facilely during electrochemical anodization.

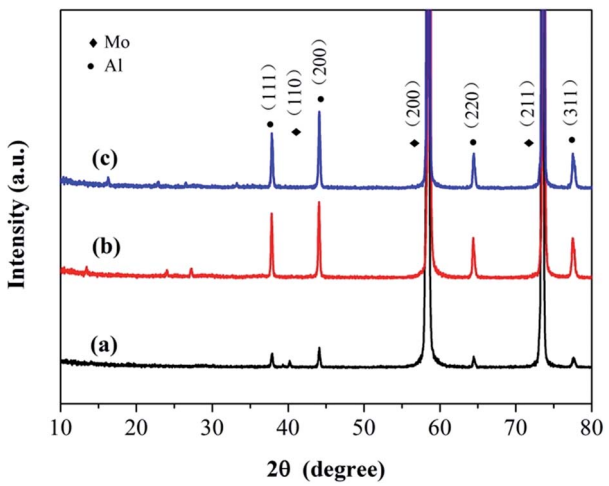

Fig. 3 XRD patterns of (a) the original Mo sheet and the anodized MoS_2 electrode prepared *via* anodization at (b) 2.0 V and (c) 2.5 V for 10 min. No resolved diffraction peaks were detected, suggesting an amorphous phase of MoS_2.

The electrocatalytic activity of the anodized MoS_2 electrodes for the HER was investigated by measuring their polarization curves in 0.5 M H_2SO_4 solution. The electrocatalytic activity was evaluated from the overpotential at a current density of 10 mA cm^{-2} (j = 10 mA cm^{-2}) for the HER. As shown in Fig. 5a, the pure Mo sheet, prior to anodization, showed a very low electrocatalytic activity for the HER. The overpotential at j = 10 mA cm^{-2} of the pure Mo sheet was 0.40 V. The low anodization voltage of 1.5 V did not obviously improve the current density because of the thin MoS_2 layer (~280 nm). However, when the pure Mo sheet was anodized at 2.0 V for 10 min (the thickness of the MoS_2 layer was ~1.2 μm), the overpotential at j = 10 mA cm^{-2} was significantly reduced to 0.31 V, which indicates that the anodized MoS_2 layer could be used as an efficient electrocatalyst for the HER. The further increase in the anodization voltage improved the electrocatalytic activity of the MoS_2 electrode because of the increase in the thickness of the MoS_2 layer. As shown in Fig. 5a, when the Mo sheet was anodized at 2.5 V for 10 min, the MoS_2 electrode (thickness = 1.6 μm) exhibited an onset potential of −0.21 V (*vs.* RHE) for the HER and a low overpotential of 0.26 V at j = 10 mA cm^{-2}. When the anodization voltage was increased to 3.0 V, the MoS_2 layer easily detached from the substrate. Although the thickness of the MoS_2 layer increased to 2.0 μm, the current density of the MoS_2 electrode decreased obviously. These results might be ascribed to the easy detachment of the MoS_2 layer during the HER.

In principle, the HER in acidic solution involves the following three possible reactions:

$$H_3O^+ + e^{1-} \rightarrow H_{ads} + H_2O \text{ (Volmer reaction)}$$

$$H_{ads} + H_{ads} \rightarrow H_2 \text{ (Tafel reaction)}$$

$$H_{ads} + H_3O^+ + e^{1-} \rightarrow H_2 + H_2O \text{ (Heyrovsky reaction)}$$

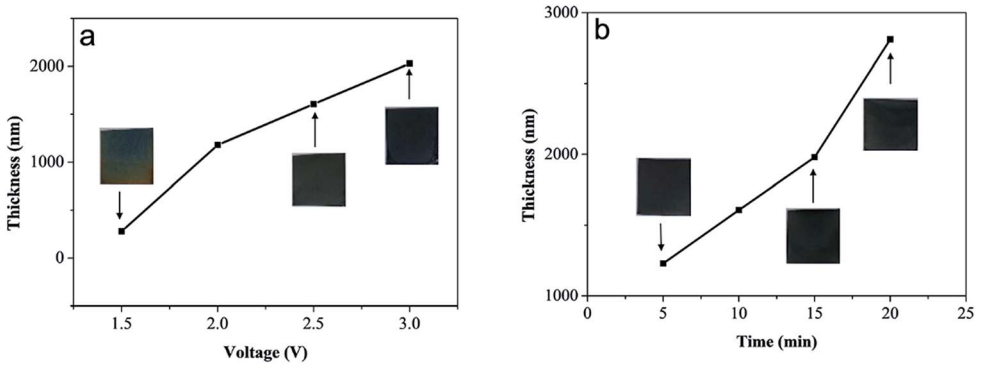

Fig. 4 The dependence of the thickness of the anodized MoS_2 layer on the (a) anodization voltage and (b) reaction time. The thickness of the MoS_2 layer increased with increasing voltage and reaction time. Inset: the corresponding photographs of the anodized MoS_2 layer.

The combination of the Volmer–Tafel or Volmer–Heyrovsky reaction can lead to the production of molecular H_2. Commonly, if the Volmer reaction is the rate-determining step for the HER, the Tafel slope is ~120 mV. However, a rate-determining step of the Heyrovsky or Tafel reaction produces a Tafel slope of ~40 or ~30 mV, respectively.[21,32,33] Therefore, based on the calculated value of the Tafel slope, we can determine the rate-determining step for the HER. From Fig. 5a, we calculated the Tafel slopes of the MoS_2 electrodes prepared *via* anodization at 1.5, 2.0 and 2.5 V for 10 min to be 93, 100 and 102 mV per decade, respectively (Fig. 5b), suggesting that they did not show a significant dependence on the anodization voltage. The Tafel slopes of our anodized MoS_2 electrodes were close to ~120 mV, which indicates that the Volmer reaction is the rate-determining step in the HER.

The electrocatalytic activity of our anodized MoS_2 electrodes for the HER could also be optimized by altering the anodization time. As shown in Fig. 5c, when the anodization voltage was fixed at 2.5 V, the increase in the anodization time enhanced the current density in the HER. However, the corresponding Tafel slope did not show a significant dependence on the anodization time (Fig. 5d). When the anodization time was 15 min, the

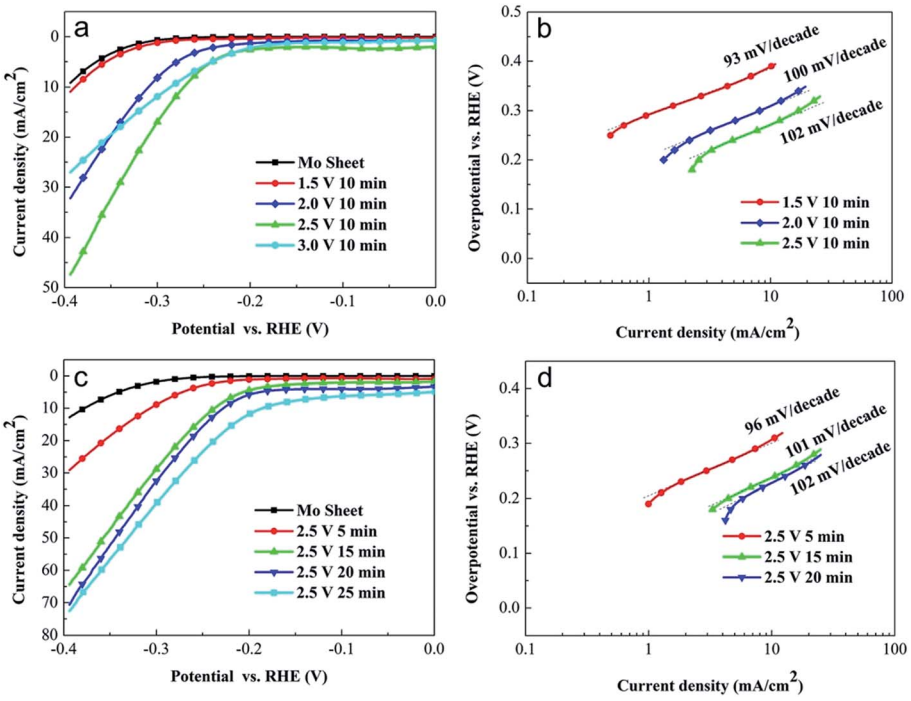

Fig. 5 (a) Polarization curves of the original Mo sheet and the MoS_2 electrodes prepared *via* anodization of the Mo sheet in Na_2S solution at 1.5, 2.0 and 2.5 V for 10 min. The current density for the HER increased with the anodization voltage. (b) The corresponding Tafel curves of the anodized MoS_2 electrodes. The MoS_2 electrode prepared *via* anodization of the Mo sheet at 2.5 V for 10 min exhibited an onset overpotential of −0.21 V (*vs.* RHE) and a Tafel slope of 102 mV per decade. (c) Polarization curves of the original Mo sheet and the MoS_2 electrodes prepared *via* anodization of the Mo sheet in Na_2S solution at 2.5 V for 5, 15, 20 and 25 min. (d) The corresponding Tafel curves. The increase in anodization time enhanced the current density in the HER. However, the Tafel slope did not show a significant dependence on the anodization time.

anodized MoS_2 electrode with a thickness of 2.0 μm demonstrated an onset potential of −0.18 V (*vs.* RHE) for the HER and an overpotential of 0.23 V at $j = 10$ mA cm^{-2}. The corresponding Tafel slope was calculated to be 101 mV per decade (Fig. 5d). The current density of this MoS_2 electrode for the HER at a potential of −0.3 V (*vs.* RHE) remained almost constant after 10 min of the HER, which indicates good stability (Fig. S3†). Note that further increasing the anodization time to 20 or 25 min did not improve the electrocatalytic activity obviously. The electrocatalytic activity of the MoS_2 electrodes prepared with different anodization times should be related to their charge transfer resistances in the HER. As shown in Fig. S4,† the original Mo metal shows a very high charge transfer resistance in the HER, which was reduced obviously by the anodization reaction. When the anodization time increased from 5 to 15 min, the charge transfer resistance of the MoS_2 electrode decreased greatly to a very low value (∼5.2 Ω) because of the increased catalytic sites, which subsequently resulted in a high electrocatalytic activity. Following the further increase in anodization time, although the thickness of the MoS_2 layer increased, the charge transfer resistance remained almost unchanged because of the excess MoS_2 catalyst, which could not make contact with the electrolyte (*i.e.* the catalytic sites are enough for the HER). Therefore, the electrocatalytic activity did not demonstrate an obvious improvement. The onset potential of −0.18 V (*vs.* RHE) for the HER in our work was comparable to that of pure MoS_2 electrodes prepared by other methods,[10,16,22–24,28,31] which indicates that our anodization strategy is an efficient route towards a high-activity MoS_2 electrode.

4. Conclusions

In summary, we have demonstrated a facile electrochemical anodization route to prepare high-activity porous MoS_2 electrodes for the HER. This anodization strategy is extraordinarily versatile, and can be used to deposit MoS_2 electrocatalysts onto the surface of Mo metal directly at room temperature and ambient pressure. The optimized MoS_2 electrodes exhibit an onset potential of −0.18 V (*vs.* RHE) for the HER, a Tafel slope of ∼101 mV per decade and an overpotential of 0.23 V at a current density of 10 mA cm^{-2} for the HER, suggesting a high electrocatalytic activity. Our results indicated that the anodization strategy is an efficient route towards high-activity MoS_2 electrodes, which may boost the application of MoS_2 electrocatalysts for the electrochemical HER.

Conflicts of interest

There are no conflicts to declare.

Acknowledgements

This work was supported by the National Basic Research Program of China (2014CB931803), the National Natural Science Foundation of China (21571011, 21701003), the China Postdoctoral Science Foundation Grant (2015M580035, 2017T100022) and the Fundamental Research Funds for the Central Universities (YWF-18-BJ-J-71).

Notes and references

1 J. A. Turner, *Science*, 2004, **305**, 972–974.
2 D. Merki and X. Hu, *Energy Environ. Sci.*, 2011, **4**, 3878–3888.
3 Y. Yin, Y. Zhang, T. Gao, T. Yao, X. Zhang, J. Han, X. Wang, Z. Zhang, P. Xu, P. Zhang, X. Cao, B. Song and S. Jin, *Adv. Mater.*, 2017, **29**, 1700311.
4 G. Zhang, G. Wang, Y. Liu, H. Liu, J. Qu and J. Li, *J. Am. Chem. Soc.*, 2016, **138**, 14686–14693.
5 Z. Seh, J. Kibsgaard, C. F. Dickens, I. Chorkendorff, J. K. Nørskov and T. F. Jaramillo, *Science*, 2017, **355**, eaad4998.
6 G. Zhang, H. Liu, J. Qu and J. Li, *Energy Environ. Sci.*, 2016, **9**, 1190–1209.
7 Y. Yin, J. Han, Y. Zhang, X. Zhang, P. Xu, Q. Yuan, L. Samad, X. Wang, Y. Wang, Z. Zhang, P. Zhang, X. Cao, B. Song and S. Jin, *J. Am. Chem. Soc.*, 2016, **138**, 7965–7972.
8 Y. Tan, P. Liu, L. Chen, W. Cong, Y. Ito, J. Han, X. Guo, Z. Tang, T. Fujita, A. Hirata and M. W. Chen, *Adv. Mater.*, 2014, **26**, 8023–8028.
9 J. Shi, D. Ma, G. Han, Y. Zhang, Q. Ji, T. Gao, J. Sun, X. Song, C. Li, Y. Zhang, X. Lang, Y. Zhang and Z. Liu, *ACS Nano*, 2014, **8**, 10196–10204.
10 Y. Yang, H. Fei, G. Ruan, C. Xiang and J. M. Tour, *Adv. Mater.*, 2014, **26**, 8163–8168.
11 J. Zhang, J. Wu, H. Guo, W. Chen, J. Yuan, U. Martinez, G. Gupta, A. Mohite, P. M. Ajayan and J. Lou, *Adv. Mater.*, 2017, **29**, 1701955.
12 S. Li, S. Wang, M. M. Salamone, A. W. Robertson, S. Nayak, H. Kim, S. C. E. Tsang, M. Pasta and J. H. Warner, *ACS Catal.*, 2017, **7**, 877–886.
13 B. Hinnemann, P. G. Moses, J. Bonde, K. P. Jørgensen, J. H. Nielsen, S. Horch, I. Chorkendorff and J. K. Nørskov, *J. Am. Chem. Soc.*, 2005, **127**, 5308–5309.
14 T. F. Jaramillo, K. P. Jørgensen, J. Bonde, J. H. Nielsen, S. Norch and I. Chorkendorff, *Science*, 2007, **317**, 100–102.
15 J. Bonde, P. G. Moses, T. F. Jaramillo, J. K. Nørskov and I. Chorkendorff, *Faraday Discuss.*, 2008, **140**, 219–231.
16 Z. Chen, D. Cummins, B. N. Reinecke, E. Clark, M. K. Sunkara and T. F. Jaramillo, *Nano Lett.*, 2011, **11**, 4168–4175.
17 J. Kibsgaard, Z. Chen, B. N. Reinecke and T. F. Jaramillo, *Nat. Mater.*, 2012, **11**, 963–969.
18 D. Kong, H. Wang, J. J. Cha, M. Pasta, K. J. Koski, J. Yao and Y. Cui, *Nano Lett.*, 2013, **13**, 1341–1347.
19 Y. Li, H. Wang, L. Xie, Y. Liang, G. Hong and H. Dai, *J. Am. Chem. Soc.*, 2011, **133**, 7296–7299.
20 J. Xie, H. Zhang, S. Li, R. Wang, X. Sun, M. Zhou, J. Zhou, X. W. Lou and Y. Xie, *Adv. Mater.*, 2013, **25**, 5807–5813.
21 Z. Lu, H. Zhang, W. Zhu, X. Yu, Y. Kuang, Z. Chang, X. Lei and X. Sun, *Chem. Commun.*, 2013, **49**, 7516–7518.
22 W. Zhou, K. Zhou, D. Hou, X. Liu, G. Li, Y. Sang, H. Liu, L. Li and S. Chen, *ACS Appl. Mater. Interfaces*, 2014, **6**, 21534–21540.

23 L. Yang, W. Zhou, J. Lu, D. Hou, Y. Ke, G. Li, Z. Tang, X. Kang and S. Chen, *Nano Energy*, 2016, **22**, 490–498.
24 L. Yang, W. Zhou, D. Hou, K. Zhou, G. Li, Z. Tang, L. Li and S. Chen, *Nanoscale*, 2015, **7**, 5203–5208.
25 C. Ma, X. Qi, B. Chen, S. Bao, Z. Yin, X. Wu, Z. Luo, J. Wei, H. Zhang and H. Zhang, *Nanoscale*, 2014, **6**, 5624–5629.
26 Y. Yan, B. Xia, N. Li, Z. Xu, A. Fisherc and X. Wang, *J. Mater. Chem. A*, 2015, **3**, 131–135.
27 X. Wang, Y. Zheng, J. Yuan, J. Shen, L. Niu and A. Wang, *Electrochim. Acta*, 2017, **235**, 422–428.
28 A. Ambrosi, Z. Sofer and M. Pumera, *Small*, 2015, **11**, 605–612.
29 S. Tan, Z. Sofer, J. Luxa and M. Pumera, *ACS Catal.*, 2016, **6**, 4594–4607.
30 Y. Chen, A. Lu, P. Lu, X. Yang, C. Jiang, M. Mariano, B. Kaehr, O. Lin, A. Taylor, I. D. Sharp, L. Li, S. S. Chou and V. Tung, *Adv. Mater.*, 2017, **29**, 1703863.
31 E. E. Benson, H. Zhang, S. A. Schuman, S. U. Nanayakkara, N. D. Bronstein, S. Ferrere, J. L. Blackburn and E. M. Miller, *J. Am. Chem. Soc.*, 2018, **140**, 441–450.
32 D. Merki, S. Fierro, H. Vrubel and X. Hu, *Chem. Sci.*, 2011, **2**, 1262–1267.
33 A. B. Laursen, P. C. K. Vesborg and I. Chorkendorff, *Chem. Commun.*, 2013, **49**, 4965–4967.
34 A. Ambrosi and M. Pumera, *ACS Catal.*, 2016, **6**, 3985–3993.
35 C. Meng, Z. Liu, T. Zhang and J. Zhai, *Green Chem.*, 2015, **17**, 2764–2768.
36 D. Gong, C. A. Grimes, O. K. Varghese, W. Hu, R. S. Singh, Z. Chen and E. C. Dickey, *J. Mater. Res.*, 2001, **16**, 3331–3334.
37 G. K. Mor, O. K. Varghese, M. Paulose, N. Mukherjee and C. A. Grimes, *J. Mater. Res.*, 2003, **18**, 2588–2593.
38 Y. R. Smith, B. Sarma, S. K. Mohanty and M. Misra, *Int. J. Hydrogen Energy*, 2013, **38**, 2062–2069.
39 R. Beranek, H. Hildebrand and P. Schmuki, *Electrochem. Solid-State Lett.*, 2003, **6**, B12–B14.
40 S. K. Mohapatra, S. E. John, S. Banerjee and M. Misra, *Chem. Mater.*, 2009, **21**, 3048–3055.
41 R. R. Rangaraju, K. S. Raja, A. Panday and M. Misra, *Electrochim. Acta*, 2010, **55**, 785–793.
42 N. Mukherjee, M. Paulose, O. K. Varghese, G. K. Mor and C. A. Grimes, *J. Mater. Res.*, 2003, **18**, 2296–2299.
43 Y. C. Nah, A. Ghicov, D. Kim and P. Schmuki, *Electrochem. Commun.*, 2008, **10**, 1777–1780.
44 M. Yang, N. K. Shrestha and P. Schmuki, *Electrochem. Commun.*, 2009, **11**, 1908–1911.
45 I. Sieber, B. Kannan and P. Schmuki, *Electrochem. Solid-State Lett.*, 2005, **8**, J10–J12.
46 I. V. Sieber and P. Schmuki, *J. Electrochem. Soc.*, 2005, **152**, C639–C644.
47 N. K. Allam, X. J. Feng and C. A. Grimes, *Chem. Mater.*, 2008, **20**, 6477–6481.
48 K. Lee and P. Schmuki, *Electrochem. Commun.*, 2011, **13**, 542–545.
49 B. Jin, X. Zhou, L. Huang, M. Lickleder, M. Yang and P. Schmuki, *Angew. Chem., Int. Ed.*, 2016, **55**, 12252–12256.
50 X. Zhou, J. Prikrylb, M. Krbalb, J. M. Macakb and P. Schmuki, *Electrochem. Commun.*, 2017, **82**, 112–116.
51 M. Yang, N. K. Shrestha and P. Schmuki, *Electrochim. Acta*, 2010, **55**, 7766–7771.
52 X. Zhou, M. Lickleder and P. Schmuki, *Electrochem. Commun.*, 2016, **73**, 33–37.
53 C. D. Wagner, W. M. Riggs, L. E. Davis, J. F. Moulder and G. E. Muilenberg, *Handbook of X-ray Photoelectron Spectroscopy, Physical Electronics Division*, Perkin-Elmer, Eden Prairie, Minnesota, 1979.
54 X. Ge, L. Chen, L. Zhang, Y. Wen, A. Hirata and M. Chen, *Adv. Mater.*, 2014, **26**, 3100–3104.
55 Y. Chang, C. Lin, T. Chen, C. Hsu, Y. Lee, W. Zhang, K. Wei and L. Li, *Adv. Mater.*, 2013, **25**, 756–760.
56 H. Vrubel, D. Merki and X. Hu, *Energy Environ. Sci.*, 2012, **5**, 6136–6144.
57 J. Kibsgaard, T. F. Jaramillo and F. Besenbacher, *Nat. Mater.*, 2014, **6**, 248–253.
58 J. D. Benck, Z. Chen, L. Y. Kuritzky, A. J. Forman and T. F. Jaramillo, *ACS Catal.*, 2012, **2**, 1916–1923.
59 T. F. Jaramillo, J. Bonde, J. Zhang, B. Ooi, K. Andersson, J. Ulstrup and I. Chorkendorff, *J. Phys. Chem. C*, 2008, **112**, 17492–17498.